

Article

Simple Method of Light Field Calculation for Shaping of 3D Light Curves

Svetlana N. Khonina ^{1,2} , Alexey P. Porfirev ^{1,2}, Sergey G. Volotovskiy ², Andrey V. Ustinov ² and Sergey V. Karpeev ^{1,2,*}

¹ Scientific Research Laboratory of Automated Systems of Scientific Research, Samara National Research University, Samara 443086, Russia; khonina@ipsiras.ru (S.N.K.); porfirev.alexey@ipsiras.ru (A.P.P.)

² Image Processing Systems Institute of RAS—Branch of the FSRC “Crystallography and Photonics” RAS, Samara 443001, Russia; sv@ipsiras.ru (S.G.V.); andr@ipsiras.ru (A.V.U.)

* Correspondence: karp@ipsiras.ru

Abstract: We propose a method for generating three-dimensional light fields with given intensity and phase distributions using purely phase transmission functions. The method is based on a generalization of the well-known approach to the design of diffractive optical elements that focus an incident laser beam into an array of light spots in space. To calculate purely phase transmission functions, we use amplitude encoding, which made it possible to implement the designed elements using a single spatial light modulator. The generation of light beams in the form of rings, spirals, Lissajous figures, and multi-petal “rose” distributions uniformly elongated along the optical axis in the required segment is demonstrated. It is also possible to control the three-dimensional structure of the intensity and phase of the shaped light fields along the propagation axis. The experimentally generated intensity distributions are in good agreement with the numerically obtained results and show high potential for the application of the proposed method in laser manipulation with nano- and microparticles, as well as in laser material processing.

Keywords: laser beam shaping; intensity; phase; Whittaker integral; Lissajous figures; transmission function



Citation: Khonina, S.N.; Porfirev, A.P.; Volotovskiy, S.G.; Ustinov, A.V.; Karpeev, S.V. Simple Method of Light Field Calculation for Shaping of 3D Light Curves. *Photonics* **2023**, *10*, 941. <https://doi.org/10.3390/photonics10080941>

Received: 8 July 2023

Revised: 28 July 2023

Accepted: 14 August 2023

Published: 17 August 2023



Copyright: © 2023 by the authors. Licensee MDPI, Basel, Switzerland. This article is an open access article distributed under the terms and conditions of the Creative Commons Attribution (CC BY) license (<https://creativecommons.org/licenses/by/4.0/>).

1. Introduction

The generation of optical fields with a given amplitude and phase distribution is a very popular task in optical manipulation [1–5] and laser material processing [6–8]. In these areas, structured laser beams with a predetermined amplitude and/or phase gradient are widely used for the realization of guiding of nano- and micro-objects [9], as well as for transfer of molten material [10,11]. For example, annular optical vortex beams with helical wave fronts are used to rotate optically trapped nano- and microparticles [5] and to implement the spiral-shaped mass transfer of a temporarily molten material in thin films of polymers [12], metals [10], and semiconductors [13]. Full control of the amplitude and phase using computer-generated holograms made it possible to implement the guiding of the trapped particles along complex two-dimensional trajectories. Because of this, various manipulation techniques and applications have been demonstrated in recent decades [2,5,8,13,14]. A further transition to the design of elements generating the required three-dimensional light fields led to the demonstration of the three-dimensional controlled guiding of microparticles in space [15]. In the field of laser material processing, light fields with a desired three-dimensional structure have been used to fabricate three-dimensional chiral microstructures [16].

There are many different techniques for the generation of structured laser beams as well as their superpositions and arrays—the use of spatial light modulators, mode convertors, and the use of nonlinear media [17–20]. In addition, there are special types of structured laser beams that are curvilinear, such as Airy beams [21]. However, to implement

full control of the beam structure, iterative or non-iterative algorithms for calculating the transmission functions of optical elements, such as diffractive optical elements (DOEs) or metasurfaces [22], should be used. In the case of the generation of two-dimensional fields, methods based on the use of two-phase DOEs calculated using the Fourier transform [9] or a rigorous mathematical derivation in the curvilinear coordinate were used [23]. Various amplitude encoding techniques combined with discrete inverse Fourier transform are also widely used to provide full intensity and phase control. However, these approaches are less efficient due to encoding [24]. Some methods include a non-iterative beam shaping technique that does not require solving inversion problems of light propagation [25]. In fact, similar approaches are used to design elements generating structured three-dimensional amplitude–phase distributions [26]. Another method, based on the use of singular beams, has made it possible to create laser beams which are navigated along parabolic, hyperbolic, or spiraling trajectories with a preserving orbital angular momentum and a nonexpanding dark “hole” in the main lobe [27]. The use of more complex approaches, including the use of two counter-propagating structured laser beams in a 4Pi focusing system, makes it possible to form both the dark hollow beams mentioned above and three-dimensional light curves with a given intensity distribution in arbitrary combinations [28]. However, the calculation is much more complicated than the methods mentioned above, and very fine tuning of the optical setup is required.

Here, we present a simple method to calculate a field for generating 3D parametric light curves based on the generalized method of focusing on a 3D set of discrete light points. In contrast to the ways mentioned above, the proposed approach provides a simple way to calculate the complex transmittance of an optical element to generate 3D light curves. In addition, we considered a way to equalize the intensity on the curve, taking into account the presence of singular points (cusps). Various types of contour distributions (rings, spirals, Lissajous figures, curves in the form of roses) are considered, and the possibility of controlling their 3D structure (such as the sequence of focusing segments of the curve at different distances due to the parametric function of the longitudinal coordinate) is demonstrated. The results of the experimental formation of the calculated curves are in good agreement with the simulation results. These pieces of research can be useful in laser manipulation with nano- and microparticles, as well as in laser material processing.

2. Methods

In this section, we discuss a method for calculating the field for the formation of 3D parametrically specified light curves based on the generalization of the focusing method in a 3D set of discrete light points.

2.1. Shaping of Parametric Light Curves: Theoretical Foundations

2.1.1. Formation of a Set of Light Points

A simple and fast solution for the formation of arbitrary light curves, including three-dimensional ones, is the composition in one optical element of several elements focusing on some primitive distributions (points, lines, rings, and others) [29–32].

Let us consider first a 2D problem. In some plane it is necessary to form a set of light points with given coordinates (u_q, v_q) and complex amplitudes (weights) g_q . If the points (primitives) do not intersect, then the field can be represented in the following form:

$$F(u, v) = \sum_q g_q \delta(u - u_q, v - v_q) \quad (1)$$

To calculate the field that forms distributions (1) in the focal plane, one can use the Fourier transform of the function defined by Equation (1):

$$\begin{aligned}
E(x, y) &= \int_{-\infty}^{\infty} \int_{-\infty}^{\infty} F(u, v) \exp\left(\frac{ik}{f}(xu + yv)\right) dudv = \\
&\int_{-\infty}^{\infty} \int_{-\infty}^{\infty} \sum_q g_q \delta(u - u_q, v - v_q) \exp\left(\frac{ik}{f}(xu + yv)\right) dudv = \\
&= \sum_q g_q \exp\left(\frac{ik}{f}(xu_q + yv_q)\right).
\end{aligned} \tag{2}$$

As follows from Equation (2), a set of prisms with carrier frequencies (u_q, v_q) is obtained. If a lens is added to the field (2), then it will form a distribution (1) in the focal plane. This approach is often used to calculate multi-order diffractive optical elements matched to a certain set of laser modes used for multiplexing and detection [33,34].

If it is necessary to form a distribution (1) in some plane at a distance z_0 from the input plane, then the Fresnel transform can be used:

$$\begin{aligned}
E(x, y) &= \int_{-\infty}^{\infty} \int_{-\infty}^{\infty} F(u, v) \exp\left[-\frac{ik}{2z_0}((x-u)^2 + (y-v)^2)\right] dudv = \\
&\sum_q g_q \exp\left[-\frac{ik}{2z_0}((x-u_q)^2 + (y-v_q)^2)\right].
\end{aligned} \tag{3}$$

In this case, a set of decentered parabolic lenses is obtained.

Using expression (3), it is easy to obtain a generalization to the 3D case:

$$E(x, y) = \sum_q g_q \exp\left[-\frac{ik}{2z_q}((x-u_q)^2 + (y-v_q)^2)\right]. \tag{4}$$

2.1.2. Formation of Parametrically Specified Light Curves

We also consider the 2D case first. Let us define the light curve in the parametric form:

$$C(u, v) = \begin{cases} u_0(t) = p_u(t), \\ v_0(t) = p_v(t), \\ t = [t_1, t_2]. \end{cases} \tag{5}$$

If the curve is thin and does not have too many intersections, then, taking into account the complex distribution of $g(t)$ along the curve, the field distribution on the plane can be represented in the following form:

$$F_t(u, v) = \int_{t_1}^{t_2} g(t) \delta(u - u_0(t), v - v_0(t)) dt. \tag{6}$$

To calculate the field that forms distribution (6) in the focal plane, one can use the Fourier transform and obtain the well-known Whittaker integral [25,35]:

$$E_t(x, y) = \int_{t_1}^{t_2} g(t) \exp\left[i \frac{k}{f}(xu_0(t) + yv_0(t))\right] dt. \tag{7}$$

When the field (7) is supplemented with a lens, curve (5) will be formed with the distribution of $g(t)$ in the focal plane. To form such a distribution in the plane at a distance z_0 , another field is used:

$$E_t(x, y) = \int_{t_1}^{t_2} g(t) \exp\left\{-i \frac{k}{2z_0}[(x - u_0(t))^2 + (y - v_0(t))^2]\right\} dt. \tag{8}$$

To generate 3D curves defined in a parametric form:

$$C(u, v, z) = \begin{cases} u(t) = p_u(t), \\ v(t) = p_v(t), \\ z(t) = p_z(t). \end{cases} \tag{9}$$

We propose the use of a generalization of expression (8) as follows:

$$F(x, y) = \int_{t_1}^{t_2} g(t) \exp \left\{ -i \frac{k}{2z(t)} [(x - u(t))^2 + (y - v(t))^2] \right\} dt. \quad (10)$$

The function $g(t)$ is complex and can be used both to introduce variations in the intensity and phase distributions along the light curve. Phase gradient control can be useful in manipulating trapped particles to create a directed energy flow along the curve [9,36,37].

2.1.3. Leveling the Intensity on the Curve by Taking into Account Singular Points (Cusps)

We also note that changes in intensity may be needed to reduce the intensity in areas where the points of the curve are denser. In this case, one can use the expression for the differential of the arc length $s(t)$ by the parameter t :

$$\frac{ds(t)}{dt} = \sqrt{\left(\frac{u(t)}{dt} \right)^2 + \left(\frac{v(t)}{dt} \right)^2}. \quad (11)$$

If the curve contains singular points (cusps), then the following relation holds at these points:

$$\frac{ds(t)}{dt} = 0. \quad (12)$$

An example is a cardioid whose radius equation is:

$$\rho(\varphi) = a(1 + \cos \varphi), \quad (13)$$

where φ is the angular parameter.

Let us take into account the relations:

$$\begin{cases} u(\varphi) = \rho(\varphi) \cos(\varphi), \\ v(\varphi) = \rho(\varphi) \sin(\varphi), \\ \rho(\varphi) = \sqrt{u^2(\varphi) + v^2(\varphi)}. \end{cases} \quad (14)$$

Then, the expression for the arc length differential in Equation (11) can be written in the following form:

$$\frac{ds(\varphi)}{d\varphi} = \sqrt{\rho^2(\varphi) + \left(\frac{d\rho(\varphi)}{d\varphi} \right)^2}. \quad (15)$$

Finally, for cardioid (13), we get:

$$\frac{ds(\varphi)}{d\varphi} = \sqrt{2a} \sqrt{1 + \cos \varphi}. \quad (16)$$

It follows from Equation (16) that at $\varphi = \pi$, there is a singular point:

$$\frac{ds(\varphi)}{d\varphi} \Big|_{\varphi=\pi} = 0. \quad (17)$$

A concentration of curve points occurs near such positions, and the intensity increases significantly in comparison with other regions of the curve. In this case, in order to compensate this concentration and smooth out the intensity distribution over the entire curve, it makes sense to set the weight function $g(t)$ in Equations (7), (8) and (10) in proportion to the function (11) or (15):

$$g(t) \cong \frac{ds(t)}{dt}. \quad (18)$$

2.2. Experimental Setup

In the experiments for the generation of the predetermined three-dimensional light curves, designed amplitude–phase transmission functions were first encoded into pure phase masks. Amplitude encoding was used to encode the calculated amplitude–phase distributions into pure phase transmission functions of the elements realized using the

SLM [38,39]. In this case, the complex amplitude–phase field $A \exp(i\phi)$ at each point was defined as the sum of two pure phase fields u and v :

$$A \exp(i\phi) = \exp(iu) + \exp(iv). \quad (19)$$

The phase values u and v are displayed in adjacent samples of the designed phase element. Phase samples u and v are in a 2×2 sub-matrix along two diagonals. The phases u and v can be calculated from the known amplitude and phase of the encoded light field as follows:

$$\begin{cases} u = \phi + \arccos(A/2), \\ v = \phi - \arccos(A/2). \end{cases} \quad (20)$$

The encoded elements were realized with a reflective phase only (with 256 gray levels) spatial light modulator (SLM) PLUTO VIS (1920×1080 -pixel resolution, $8 \mu\text{m}$ pixel pitch). The experimental setup is shown in Figure 1. The output laser beam with a wavelength of $\lambda = 532 \text{ nm}$ was extended and collimated with a system composed of a pinhole PH (aperture size of $40 \mu\text{m}$) and a lens L1 ($f_1 = 250 \text{ mm}$). Diaphragm D1 was used to separate the central spot of the Airy disk resulting from the wave diffraction of the pinhole. Then, after the modulated laser beam reflected from the SLM was spatially filtered with the help of a diaphragm, D2, and two lenses, L2 and L3, with focal lengths of $f_2 = 500 \text{ mm}$ and $f_3 = 150 \text{ mm}$. This combination of lenses also formed an image of the plane conjugated to the SLM display in the focal plane of lens L3. The intensity distributions of the investigated laser beams formed at various distances from the plane $z = 0$ were captured with a video camera CAM (TOUPCAM UHCCD00800KPA, Hangzhou TouTek Photonics Co., Ltd., Hangzhou, China, 3264×2448 pixels) mounted on the optical rail.

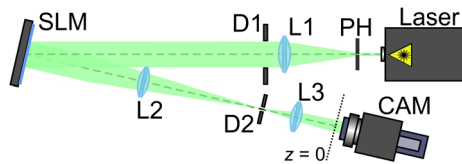


Figure 1. Experimental setup for generation of predetermined three-dimensional light curves: laser is a solid-state laser, PH is a pinhole (aperture size of $40 \mu\text{m}$); L1, L2, and L3 are lenses ($f_1 = 250$, $f_2 = 500$, and $f_3 = 150 \text{ mm}$, respectively), D1 and D2 are circular diaphragms, SLM is a spatial light modulator (HOLOEYE PLUTO VIS with a 1920×1080 -pixel resolution, HOLOEYE Photonics AG, Berlin, Germany), and CAM is a video camera (TOUPCAM UHCCD00800KPA, 3264 \times 2448 pixels).

3. Results

In this section, we present the results of the simulation and experiment for the following general parameters: $k = 2\pi/\lambda$, $\lambda = 532 \text{ nm}$. The remaining parameters were varied in accordance with the defined curves and the field distribution on them.

3.1. Light Ring

To form a 2D ring in a defined plane z_0 , the following parametric expression is used:

$$C_r(u, v, z) = \begin{cases} u(t) = r_c \cos(t), \\ v(t) = r_c \sin(t), \\ z(t) = z_0. \end{cases} \quad (21)$$

We used $z_0 = 250 \text{ mm}$, $r_c = 0.5 \text{ mm}$, $t \in [0, 2\pi]$, $g(t) = 1$ (the intensity is uniform along the curve). The results of the calculation and experiment are shown in Figure 2. As can be seen, a clear formation of the ring occurs at a distance $z = z_0 = 250 \text{ mm}$ (before and after this plane, the picture looks blurry).

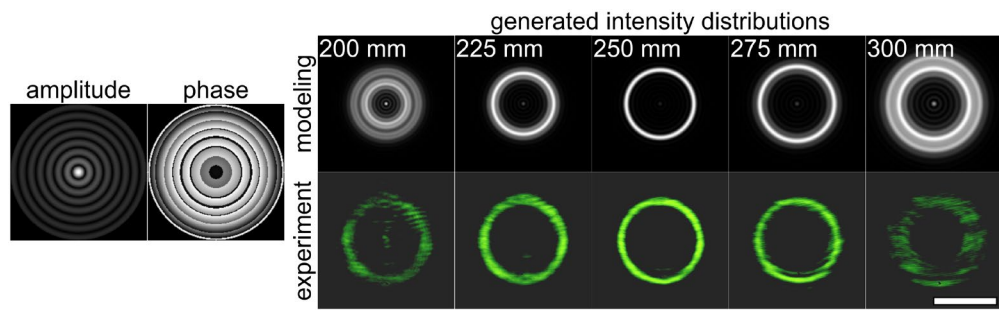


Figure 2. Shaping of a 2D light ring at the distance $z_0 = 250$ mm: modeling (upper line) and experimentally obtained (bottom line) intensity distributions at various distances from the plane $z = 0$ (amplitude and phase are shown on the left). The scale bar is 1 mm. The calculated amplitude and phase distributions used for the generation of the 2D light ring refer to the source plane ($z = 0$ mm).

To form a 3D curve in the form of an open and stretched ring along the axis on the interval $z \in [z_s, z_e]$, the following parametric expression is used:

$$C_{3D_r}(u, v, z) = \begin{cases} u(t) = r_c \cos(t), \\ v(t) = r_c \sin(t), \\ z(t) = z_s + t \cdot (z_e - z_s)/2\pi. \end{cases} \quad (22)$$

with $r_c = 0.5$ mm, $t \in [0, 2\pi]$, $g(t) = 1$, $z_s = 200$ mm, and $z_e = 300$ mm.

The results of the calculation and experiment are shown in Figure 3. As can be seen, different segments of the ring are sequentially focused at different distances. Note, the radius of the 3D ring slightly increases with an increasing distance, i.e., in fact, a spiral distribution is formed.

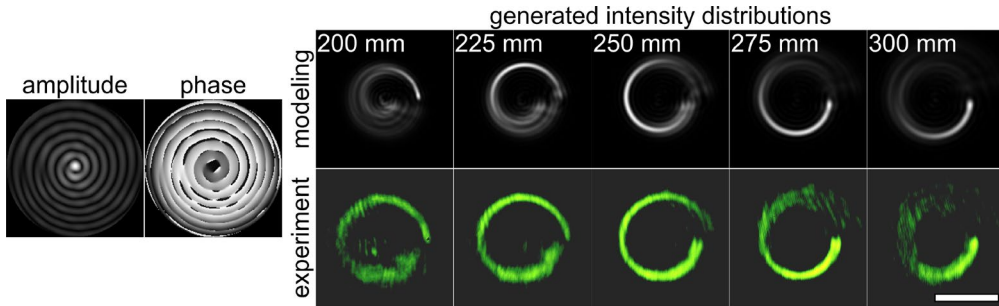


Figure 3. Shaping of a 3D ring uniformly stretched along the optical axis on the interval $z \in [200 \text{ mm}, 300 \text{ mm}]$: modeling (upper line) and experimentally obtained (bottom line) intensity distributions at various distances from the plane $z = 0$ (amplitude and phase are shown on the left). The scale bar is 1 mm. The calculated amplitude and phase distributions used for the generation of the 3D light ring refer to the source plane ($z = 0$ mm).

3.2. Light Spiral

To form a 2D light spiral with two turns at a defined plane z_0 , the following parametric expression is used:

$$C_s(u, v, z) = \begin{cases} u(t) = r_c \cdot t \cdot \cos(t)/4\pi, \\ v(t) = r_c \cdot t \cdot \sin(t)/4\pi, \\ z(t) = z_0. \end{cases} \quad (23)$$

with $r_c = 1$ mm, $t \in [0, 4\pi]$, $g(t) = t$ (the function grows towards the periphery of the curve to provide a uniform intensity due to the growth of the radius of the curve).

The results of the calculation and experiment are shown in Figure 4, which shows a clear formation of a two-turn spiral with uniform intensity at a distance $z = z_0 = 250$ mm (the picture is blurry before and after this plane).

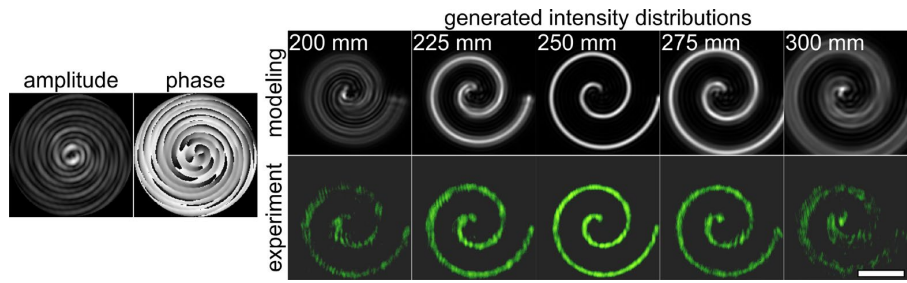


Figure 4. Shaping of a 2D light spiral with two turns in a plane $z_0 = 250$ mm (the rest as in Figure 1).

To form a 3D two-turn spiral uniformly stretched along the optical axis on the interval $z \in [z_s, z_e]$, the following parametric expression is used:

$$C_{3D_s}(u, v, z) = \begin{cases} u(t) = r_c \cdot t \cdot \cos(t)/4\pi, \\ v(t) = r_c \cdot t \cdot \sin(t)/4\pi, \\ z(t) = z_s + t \cdot (z_e - z_s)/4\pi. \end{cases} \quad (24)$$

with $r_c = 1$ mm, $t \in [0, 4\pi]$, $g(t) = t$, $z_s = 200$ mm, and $z_e = 300$ mm.

In this case, when moving from z_s to z_e , the spiral will “appear” from the center to the periphery (Figure 5). If $z(t) = z_e - t(z_e - z_s)/4\pi$, then it will be vice versa—the spiral will “appear” from the periphery to the center (Figure 6). Note, a different scenario for focusing parts of the curve can be useful for capturing and transporting microparticles to different regions of space.

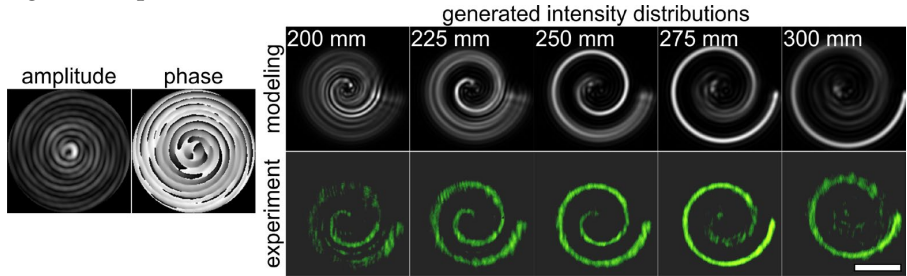


Figure 5. Shaping of a 3D light two-turn spiral uniformly stretched along the optical axis on interval $z \in [200 \text{ mm}, 300 \text{ mm}]$ with direction from the center to the periphery of the curve (the rest as in Figure 2).

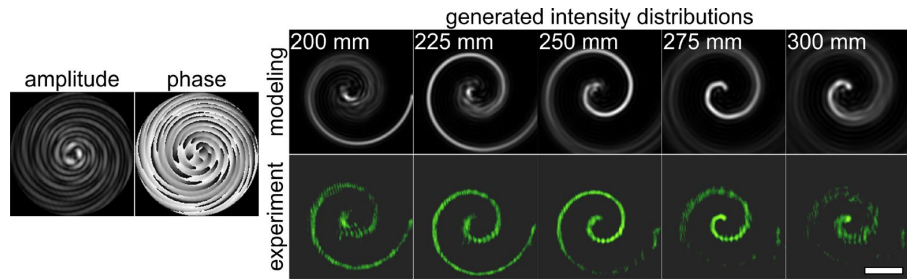


Figure 6. Shaping of a 3D light two-turn spiral uniformly stretched along the optical axis on a segment $z \in [200 \text{ mm}, 300 \text{ mm}]$ with direction from the periphery to the center of the curve (the rest as in Figure 2).

3.3. Lissajous Figures

To form 2D Lissajous figures in a defined plane z_0 , the following parametric expression is used:

$$C_L(u, v, z) = \begin{cases} u(t) = r_u \cdot \cos(m_1 t), \\ v(t) = r_v \cdot \sin(m_2 t), \\ z(t) = z_0. \end{cases} \quad (25)$$

with $t \in [0, 2\pi]$, m_1 and m_2 are integers specifying the order of the Lissajous figure [40].

Although curves of this type do not have cusps, there are regions with increased points density. To reduce the increase in intensity in these areas, one can use the weighting function $g(t)$, which is proportional to the arc length differential, using expression (11):

$$g(t) \cong \frac{ds(t)}{dt} = \sqrt{[r_u m_1 \sin(m_1 t)]^2 + [r_v m_2 \cos(m_2 t)]^2}. \quad (26)$$

The results of calculation and experiment for various parameters are shown in Figure 7. As can be seen, the function $g(t)$ makes it possible to significantly change the intensity distribution, as well as to introduce a phase gradient along the curve.

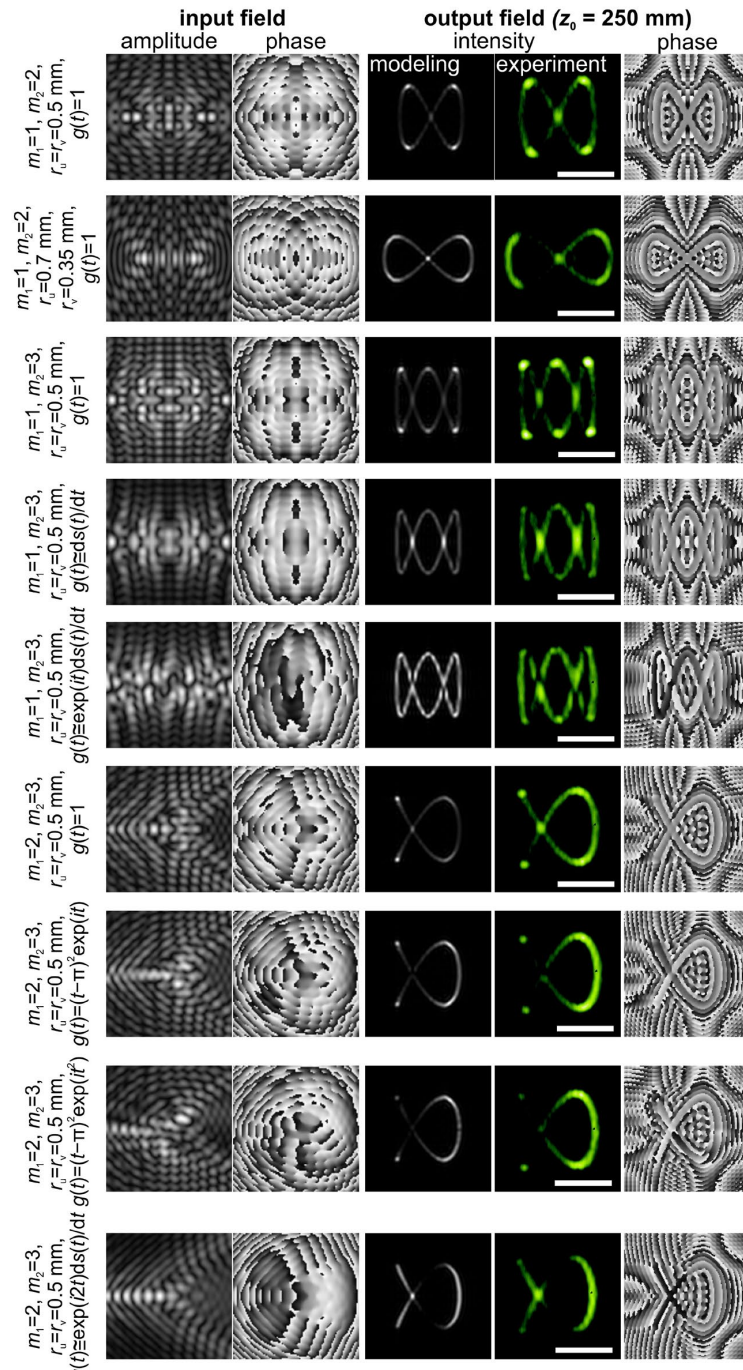


Figure 7. Modeling and experimentally obtained intensity distributions of 2D Lissajous figures at the distance z_0 . The scale bar is 1 mm. The calculated amplitude and phase distributions used for the generation of the 2D Lissajous figures refer to the source plane ($z = 0 \text{ mm}$).

Note, for the Lissajous figure with $m_1 = 1, m_2 = 3$, the use of the weight function of Equation (24) made it possible to equalize the intensity along the curve (compare the third and four lines of Figure 7). There are two brighter points due to the fact that these points are passed twice for different values of the parameter.

The use of the complex function $g(t)$ makes it possible to introduce a phase gradient of different directions and speeds (the last four lines of Figure 7).

To form 3D Lissajous figures uniformly stretched along the optical axis on the interval $z \in [z_s, z_e]$, the following parametric expression is used:

$$C_{3D_L}(u, v, z) = \begin{cases} u(t) = r_c \cdot \cos[m_1(t + t_0)], \\ v(t) = r_c \cdot \sin[m_2(t + t_0)], \\ z(t) = z_s + t \cdot (z_e - z_s)/2\pi. \end{cases} \quad (27)$$

with $r_c = 0.5$ mm, $t \in [0, 2\pi]$, $g(t) = 1$, $z_s = 200$ mm, and $z_e = 300$ mm.

The results of the calculation and experiment are shown in Figures 8 and 9 with different starting/ending points on the curve which are controlled by t_0 .

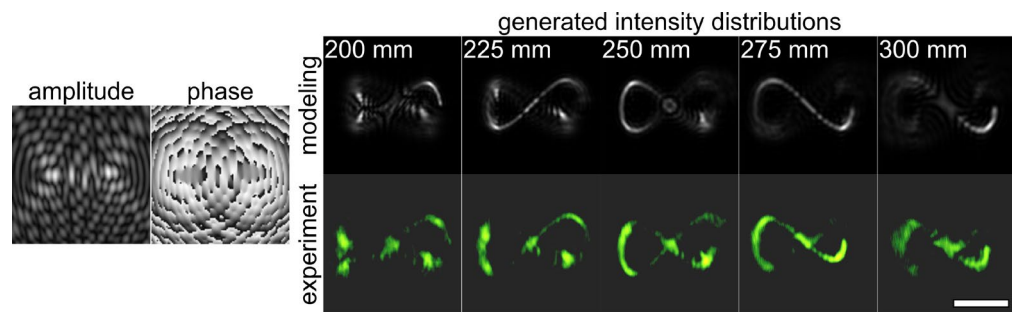


Figure 8. Shaping of a 3D Lissajous figure with parameters $m_1 = 1, m_2 = 2, g(t) = 1$, uniformly stretched along the optical axis on the interval $z \in [200 \text{ mm}, 300 \text{ mm}]$ with $t_0 = 0$. The calculated amplitude and phase distributions used for the generation of the 3D Lissajous figures refer to the source plane ($z = 0 \text{ mm}$).

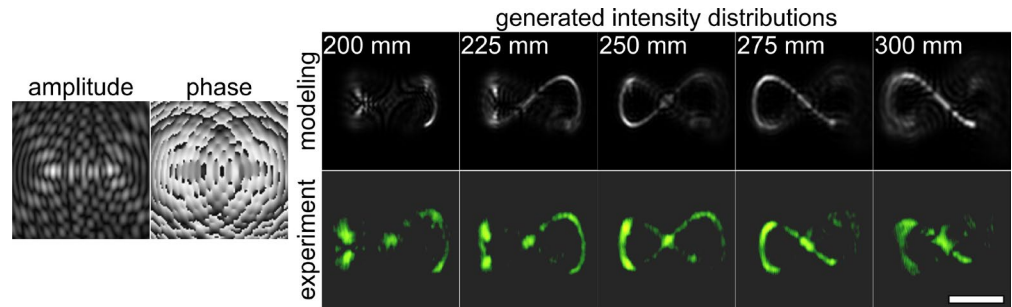


Figure 9. Shaping of a 3D Lissajous figure with parameters $m_1 = 1, m_2 = 2, g(t) = 1$ uniformly stretched along the optical axis on the interval $z \in [200 \text{ mm}, 300 \text{ mm}]$ with $t_0 = \pi/4$. The calculated amplitude and phase distributions used for the generation of the 3D Lissajous figures refer to the source plane ($z = 0 \text{ mm}$).

3.4. Rose Curves

To form 2D m -petal “roses” in a defined plane z_0 , the following parametric expression is used:

$$C_{rs}(u, v, z) = \begin{cases} u(t) = r_c \cdot \cos(mt) \cos(t), \\ v(t) = r_c \cdot \cos(mt) \sin(t), \\ z(t) = z_0. \end{cases} \quad (28)$$

with $r_c = 0.7$ mm, m is a parameter, which in the general case can be a non-integer, which allows you to form “double” roses.

The results of the calculation and experiment are shown in Figure 10.

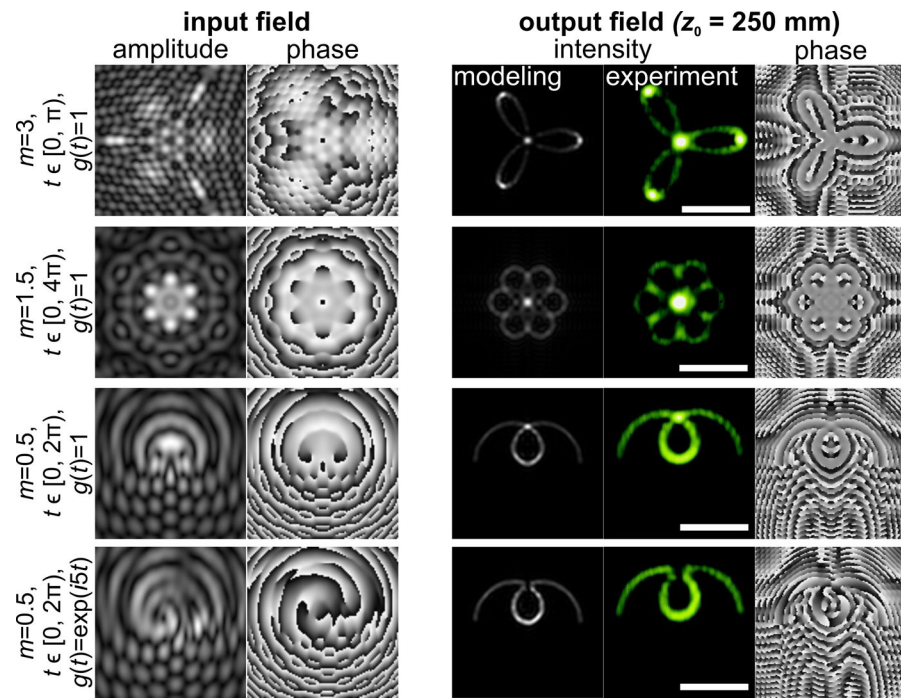


Figure 10. Modeling and experimentally obtained intensity distributions of 2D “rose” curves at the distance z_0 . The scale bar is 1 mm. The calculated amplitude and phase distributions used for the generation of the 2D “rose” curves refer to the source plane ($z = 0$ mm).

The issue of increased brightness of self-intersection points is especially important for rose curves, in which the multiplicity of the central point is equal to the number of petals. In this case, using the weight function of Equation (18) will not help.

However, inserting a phase shift (such as $g(t) = \exp(i\alpha t)$) made it possible to remove a bright light point through which the curve passes twice due to destructive interference (compare the third and fourth lines in Figure 10).

To form 3D rose curves uniformly stretched along the optical axis on the interval $z \in [z_s, z_e]$, the following parametric expression is used:

$$C_{3D_rs}(u, v, z) = \begin{cases} u(t) = r_c \cdot \cos(mt) \cos(t), \\ v(t) = r_c \cdot \cos(mt) \sin(t), \\ z(t) = z_s + t \cdot (z_e - z_s) / 2\pi. \end{cases} \quad (29)$$

with $r_c = 0.7$ mm, $z_s = 200$ mm, and $z_e = 300$ mm. The results of the calculation and experiment are shown in Figures 11 and 12.

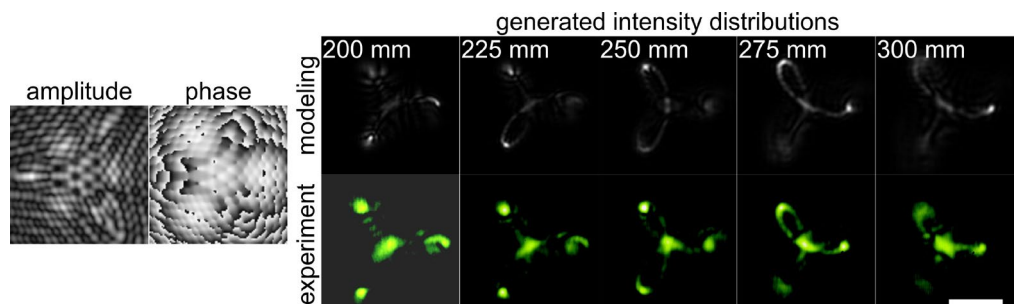


Figure 11. Modeling and experimentally obtained intensity distributions of a 3D curve in the form of a 3-petal “rose” with parameters $m = 3$, $t \in [0, \pi]$ uniformly stretched along the optical axis on the interval $z \in [200 \text{ mm}, 300 \text{ mm}]$ (the rest as in Figure 2).

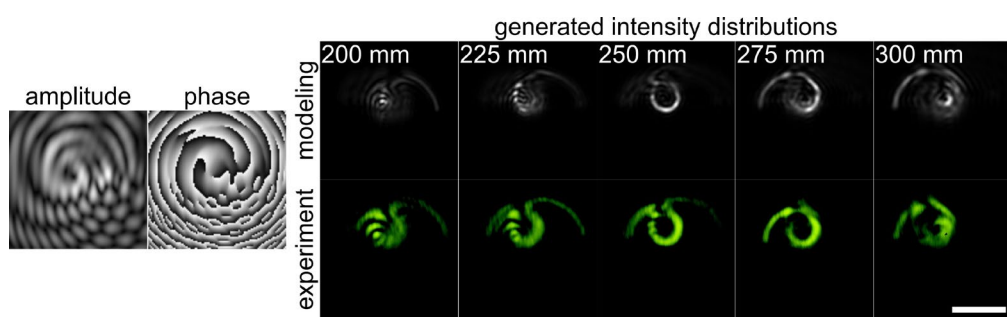


Figure 12. Modeling and experimentally obtained intensity distributions of a 3D curve in the form of a part of a “rose” $m = 0.5$, $t \in [0, 2\pi]$ with a linear phase shift along the curve $g(t) = \exp(i5t)$ uniformly stretched along the optical axis on a segment $z \in [200 \text{ mm}, 300 \text{ mm}]$ (the rest as in Figure 2).

It can be seen that in the case of the formation of 3D curves (Figures 3, 5, 6, 8, 9, 11 and 12) at different distances, separate parts (segments) are most clearly distinguished and focused on accordance with the equation for the dependence $z(t)$.

As can be seen from the above presented simulation and experimental results, there is good agreement between them. This fact shows that the use of a gray scale SLM in combination with the coding method described in Section 2.2 provides a sufficient quality of the optical realization of the given 3D intensity distributions.

4. Discussion

In this work, we presented a simple approach that can be used to calculate the transmission functions of diffractive optical elements shaping three-dimensional laser beams with predetermined intensity and phase distributions on an arbitrary segment of propagation. The approach is non-iterative, does not require high-performance computing, and makes it easy to control not only the trajectory of the beam propagation but also the uniformity and direction of the intensity gradient along the generated light curve.

One major feature of the proposed method from the previously described methods [15,16,25–27] is the weighting function, which takes into account not only the desired distribution of intensity and phase along the curve, but also provides its correction considering the nonlinearity of the curve equation (described in detail in Section 2.1.3). Note that such a correction is useful for a wide range of curves, including those without singular points. For example, without such a correction, the unit amplitude weight function $g(t) = 1$ does not provide a uniform intensity on a spiral (since the intensity will decrease as it unwinds). More clearly the action of the correction can be seen on the Lissajous curves (Figure 7, rows 3 and 4).

It is worth mentioning that the construction of a curve by points (using the considered method) suggests that they should be set densely enough so that unevenness does not visually appear. This complicates the required transmission function by having a fine structure. Therefore, for the formation of some types of curves (for example, spirals) it may be more convenient to use generalized spiral axicons or lenses [41–45]. However, such spiral elements are suitable mainly for curves described by a single-valued function. Therefore, we advise the generation of a “terry rose” by the method proposed in this work. The reason is that the curve parameter, even if it has the meaning of an angle, can take any different value, and the geometric angle is cyclic in 2π radians.

In addition, it was shown in this work that the additional phase function provides the intensity distribution manipulation in the vicinity of the self-intersection points of the curves (Figure 10, lines 3 and 4).

The advantages of the proposed method mentioned above are useful in laser manipulation and laser material processing since it can be used to control the direction of movement of optically trapped nano- and microparticles and temporarily molten materials on the surface of thin films. In the case of the laser processing of bulk materials, this can also

be used to provide additional control over the three-dimensional structure of the formed chiral microstructures [16].

The limitation of the proposed method is due to the non-high efficiency of generating the desired laser beams, which can be explained by the need to perform additional amplitude encoding the implementation of a purely phase transmission function. However, this advantage can be easily overcome by using high-power laser sources and fabricating the designed elements by etching glass or fused silica substrates.

5. Conclusions

A method for generating three-dimensional light fields with given intensity and phase distributions using purely phase transmission functions was proposed and numerically and experimentally investigated. The method is based on a generalization of the well-known approach to the design of diffractive optical elements that focus an incident laser beam into an array of light spots in space. The possibilities of generating curved light beams in the form of rings and spirals uniformly elongated along the optical axis in the required segment were shown. In this case, we can control the number of turns of the generated light spirals, as well as the dimensions of the generated light distributions. In addition, the possibility of generating light fields in the form of Lissajous figures and multi-petal “rose” distributions was demonstrated. The proposed approach can be used to control the three-dimensional structure of the intensity and phase of shaped light fields along the propagation axis. All these examples of light fields were successfully generated experimentally, which indicates the high applicability of the proposed approach.

Author Contributions: Conceptualization: S.N.K.; methodology, S.N.K. and S.V.K.; software, S.G.V.; validation, S.N.K., A.P.P. and A.V.U.; formal analysis, S.N.K., A.V.U. and A.P.P.; investigation, A.P.P., S.N.K. and A.V.U.; resources, S.G.V.; data curation, S.N.K. and A.P.P.; writing—original draft preparation, S.N.K., A.P.P., A.V.U. and S.V.K.; writing—review and editing, S.N.K. and A.P.P.; visualization, A.P.P. and S.N.K.; supervision, S.V.K.; project administration, S.V.K.; funding acquisition, S.V.K. All authors have read and agreed to the published version of the manuscript.

Funding: This work was supported by the Russian Science Foundation under Grant No. 22-12-00041.

Institutional Review Board Statement: Not applicable.

Informed Consent Statement: Not applicable.

Data Availability Statement: Data will be made available on request.

Conflicts of Interest: The authors declare no conflict of interest.

References

1. Kritzinger, A.; Forbes, A.; Forbes, P.B.C. Optical Trapping and Fluorescence Control with Vectorial Structured Light. *Sci. Rep.* **2022**, *12*, 17690. [[CrossRef](#)] [[PubMed](#)]
2. Otte, E.; Denz, C. Optical Trapping Gets Structure: Structured Light for Advanced Optical Manipulation. *Appl. Phys. Rev.* **2020**, *7*, 041308. [[CrossRef](#)]
3. Zhou, L.M.; Shi, Y.; Zhu, X.; Hu, G.; Cao, G.; Hu, J.; Qiu, C.W. Recent Progress on Optical Micro/Nanomanipulations: Structured Forces, Structured Particles, and Synergetic Applications. *ACS Nano* **2022**, *16*, 13264–13278. [[CrossRef](#)] [[PubMed](#)]
4. Singh, B.K.; Nagar, H.; Roichman, Y.; Arie, A. Particle Manipulation Beyond the Diffraction Limit Using Structured Super-Oscillating Light Beams. *Light Sci. Appl.* **2017**, *6*, e17050. [[CrossRef](#)]
5. Yang, Y.; Ren, Y.X.; Chen, M.; Arita, Y.; Rosales-Guzmán, C. Optical Trapping with Structured Light: A Review. *Adv. Photon.* **2021**, *3*, 034001.
6. Flamm, D.; Grossmann, D.G.; Sailer, M.; Kaiser, M.; Zimmermann, F.; Chen, K.; Jenne, M.; Kleiner, J.; Hellstern, J.; Tillkorn, C.; et al. Structured Light for Ultrafast Laser Micro-and Nanoprocessing. *Opt. Eng.* **2021**, *60*, 025105. [[CrossRef](#)]
7. Malinauskas, M.; Žukauskas, A.; Hasegawa, S.; Hayasaki, Y.; Mizeikis, V.; Buividas, R.; Juodkazis, S. Ultrafast Laser Processing of Materials: From Science to Industry. *Light Sci. Appl.* **2016**, *5*, e16133. [[CrossRef](#)]
8. Porfirev, A.; Khonina, S.; Kuchmizhak, A. Light–Matter Interaction Empowered by Orbital Angular Momentum: Control of Matter at the Micro-and Nanoscale. *Prog. Quantum. Electron.* **2023**, *88*, 100459. [[CrossRef](#)]
9. Jesacher, A.; Maurer, C.; Schwaighofer, A.; Bernet, S.; Ritsch-Marte, M. Full Phase and Amplitude Control of Holographic Optical Tweezers with High Efficiency. *Opt. Express* **2008**, *16*, 4479–4486. [[CrossRef](#)]

10. Syubaev, S.; Zhizhchenko, A.; Kuchmizhak, A.; Porfirev, A.; Pustovalov, E.; Vitrik, O.; Kulchin, Y.; Khonina, S.; Kudryashov, S. Direct Laser Printing of Chiral Plasmonic Nanojets by Vortex Beams. *Opt. Express* **2017**, *25*, 10214–10223. [CrossRef]
11. Syubaev, S.; Porfirev, A.; Zhizhchenko, A.; Vitrik, O.; Kudryashov, S.; Fomchenkov, S.; Khonina, S.; Kuchmizhak, A. Zero-Orbital-Angular-Momentum Laser Printing of Chiral Nanoneedles. *Opt. Lett.* **2017**, *42*, 5022–5025. [CrossRef] [PubMed]
12. Ambrosio, A.; Marrucci, L.; Borbone, F.; Roviello, A.; Maddalena, P. Light-Induced Spiral Mass Transport in Azo-Polymer Films under Vortex-Beam Illumination. *Nat. Commun.* **2013**, *3*, 989. [CrossRef]
13. Takahashi, F.; Miyamoto, K.; Hidai, H.; Yamane, K.; Morita, R.; Omatsu, T. Picosecond Optical Vortex Pulse Illumination Forms a Monocrystalline Silicon Needle. *Sci. Rep.* **2016**, *6*, 21738. [CrossRef] [PubMed]
14. Dholakia, K.; Lee, W.M. Optical Trapping Takes Shape: The Use of Structured Light Fields. *Adv. At. Mol. Opt. Phys.* **2008**, *56*, 261–337.
15. Rodrigo, J.A.; Alieva, T. Freestyle 3D Laser Traps: Tools for Studying Light-Driven Particle Dynamics and Beyond. *Optica* **2015**, *2*, 812–815. [CrossRef]
16. Ni, J.; Wang, C.; Zhang, C.; Hu, Y.; Yang, L.; Lao, Z.; Xu, B.; Li, J.; Wu, D.; Chu, J. Three-Dimensional Chiral Microstructures Fabricated by Structured Optical Vortices in Isotropic Material. *Light Sci. Appl.* **2017**, *6*, e17011. [CrossRef]
17. Huang, T.D.; Lu, T.H. Controlling an Optical Vortex Array from a Vortex Phase Plate, Mode Converter, and Spatial Light Modulator. *Opt. Lett.* **2019**, *44*, 3917–3920. [CrossRef]
18. Shen, S.; Yang, Z.; Li, X.; Zhang, S. Periodic Propagation of Complex-Valued Hyperbolic-Cosine-Gaussian Solitons and Breathers with Complicated Light Field Structure in Strongly Nonlocal Nonlinear Media. *Commun. Nonlinear Sci. Numer. Simul.* **2021**, *103*, 106005. [CrossRef]
19. Xu, J.; Liu, Z.; Pan, K.; Zhao, D. Asymmetric Rotating Array Beams with Free Movement and Revolution. *Chin. Opt. Lett.* **2022**, *20*, 022602. [CrossRef]
20. Song, L.-M.; Yang, Z.-J.; Li, X.-L.; Zhang, S.-M. Coherent Superposition Propagation of Laguerre–Gaussian and Hermite–Gaussian Solitons. *Appl. Math. Lett.* **2020**, *102*, 106114. [CrossRef]
21. Efremidis, N.K.; Chen, Z.; Segev, M.; Christodoulides, D.N. Airy Beams and Accelerating Waves: An Overview of Recent Advances. *Optica* **2019**, *6*, 686–701. [CrossRef]
22. Lee, G.-Y.; Yoon, G.; Lee, S.-Y.; Yun, H.; Cho, J.; Lee, K.; Kim, H.; Rho, J.; Lee, D. Complete Amplitude and Phase Control of Light Using Broadband Holographic Metasurfaces. *Nanoscale* **2018**, *10*, 4237–4245. [CrossRef] [PubMed]
23. Chen, Y.; Wang, T.; Ren, Y.; Fang, Z.; Ding, G.; He, L.; Lu, R.; Huang, K. Generalized Perfect Optical Vortices Along Arbitrary Trajectories. *J. Phys. D Appl. Phys.* **2021**, *54*, 214001. [CrossRef]
24. Tang, X.; Nan, F.; Yan, Z. Rapidly and Accurately Shaping the Intensity and Phase of Light for Optical Nano-Manipulation. *Nanoscale Adv.* **2020**, *2*, 2540–2547. [CrossRef] [PubMed]
25. Rodrigo, J.A.; Alieva, T. Polymorphic Beams and Nature Inspired Circuits for Optical Current. *Sci. Rep.* **2016**, *6*, 35341. [CrossRef] [PubMed]
26. Rodrigo, J.A.; Alieva, T.; Abramochkin, E.; Castro, I. Shaping of Light Beams Along Curves in Three Dimensions. *Opt. Express* **2013**, *21*, 20544–20555. [CrossRef] [PubMed]
27. Zhao, J.; Chremmos, I.D.; Song, D.; Christodoulides, D.N.; Efremidis, N.K.; Chen, Z. Curved Singular Beams for Three-Dimensional Particle Manipulation. *Sci. Rep.* **2015**, *5*, 12086. [CrossRef] [PubMed]
28. Yan, S.; Yu, X.; Li, M.; Yao, D. Curved Optical Tubes in a 4Pi Focusing System. *Opt. Express* **2015**, *23*, 22890–22897. [CrossRef] [PubMed]
29. Khonina, S.N.; Koltyar, V.V.; Soifer, V.A. Techniques for Encoding Composite Diffractive Optical Elements. *Proc. SPIE* **2003**, *5036*, 493–498.
30. Doskolovich, L.L.; Dmitriev, A.Y.; Bezus, E.A.; Moiseev, M.A. Analytical Design of Freeform Optical Elements Generating an Arbitrary-Shape Curve. *Appl. Opt.* **2013**, *52*, 2521–2526. [CrossRef]
31. Vijayakumar, A.; Bhattacharya, S. Design, Fabrication and Evaluation of Diffractive Optical Elements for Generation of Focused Ring Patterns. *Proc. SPIE* **2015**, *9449*, 944902.
32. Khorin, P.A.; Porfirev, A.P.; Khonina, S.N. Composite Diffraction-Free Beam Formation Based on Iteratively Calculated Primitives. *Micromachines* **2023**, *14*, 989. [CrossRef] [PubMed]
33. Wang, Z.; Zhang, N.; Yuan, X.-C. High-Volume Optical Vortex Multiplexing and Demultiplexing for Free-Space Optical Communication. *Opt. Express* **2011**, *19*, 482–492. [CrossRef] [PubMed]
34. Kazanskiy, N.L.; Khonina, S.N.; Karpeev, S.V.; Porfirev, A.P. Diffractive Optical Elements for Multiplexing Structured Laser Beams. *Quantum Electron.* **2020**, *50*, 629–635. [CrossRef]
35. Ortiz-Ambriz, A.; Lopez-Aguayo, S.; Kartashov, Y.V.; Vysloukh, V.A.; Petrov, D.; Garcia-Gracia, H.; Gutierrez-Vega, J.C.; Torner, L. Generation of Arbitrary Complex Quasi-Non-Diffracting Optical Patterns. *Opt. Express* **2013**, *21*, 22221–22231. [CrossRef]
36. Bekshaev, A.Y.; Soskin, M.S. Transverse Energy Flows in Vectorial Fields of Paraxial Beams with Singularities. *Opt. Commun.* **2007**, *271*, 332–348. [CrossRef]
37. Bekshaev, A.Y. Internal Energy Flows and Instantaneous Field of a Monochromatic Paraxial Light Beam. *Appl. Opt.* **2012**, *51*, C13–C16. [CrossRef]
38. Goorden, A.; Bertolotti, J.; Mosk, A.P. Superpixel-Based Spatial Amplitude and Phase Modulation Using a Digital Micromirror Device. *Opt. Express* **2014**, *22*, 17999–18009. [CrossRef]

39. Kovalev, A.A.; Kotlyar, V.V.; Porfirev, A.P. Generation of Half-Pearcey Laser Beams by a Spatial Light Modulator. *Comput. Opt.* **2014**, *38*, 658–662. [[CrossRef](#)]
40. Kessler, D.A.; Freund, I. Lissajous singularities. *Opt. Lett.* **2003**, *28*, 111–113. [[CrossRef](#)]
41. Alonzo, C.A.; Rodrigo, P.J.; Glückstad, J. Helico-Conical Optical Beams: A Product of Helical and Conical Phase Fronts. *Opt. Express* **2005**, *13*, 1749–1760. [[CrossRef](#)] [[PubMed](#)]
42. Cheng, S.B.; Xia, T.; Liu, M.S.; Jin, Y.Y.; Zhang, G.; Tao, S.H. Power-Exponent Helico-Conical Optical Beams. *Opt. Laser Technol.* **2019**, *117*, 288–292. [[CrossRef](#)]
43. Khonina, S.N.; Ustinov, A.V.; Logachev, V.I.; Porfirev, A.P. Properties of Vortex Light Fields Generated by Generalized Spiral Phase Plates. *Phys. Rev. A* **2020**, *101*, 043829. [[CrossRef](#)]
44. Xia, T.; Tao, S.H.; Cheng, S.B. A Spiral-Like Curve with an Adjustable Opening Generated by a Modified Helico-Conical Beam. *Opt. Commun.* **2020**, *458*, 124824. [[CrossRef](#)]
45. Khonina, S.N.; Ustinov, A.V.; Porfirev, A.P. Diatom Optical Element: A Quantized Version of the Generalized Spiral Lens. *Opt. Lett.* **2022**, *47*, 3988–3991. [[CrossRef](#)]

Disclaimer/Publisher’s Note: The statements, opinions and data contained in all publications are solely those of the individual author(s) and contributor(s) and not of MDPI and/or the editor(s). MDPI and/or the editor(s) disclaim responsibility for any injury to people or property resulting from any ideas, methods, instructions or products referred to in the content.